

Just a Momentum: Analytical Study of Momentum-Based Acceleration Methods in Paradigmatic High-Dimensional Non-Convex Problems

Stefano Sarao Mannelli^{1,*} and Pierfrancesco Urbani^{2,†}

¹Department of Experimental Psychology, University of Oxford, Oxford, United Kingdom

²Université Paris-Saclay, CNRS, CEA, Institut de physique théorique, 91191, Gif-sur-Yvette, France

When optimizing over loss functions it is common practice to use momentum-based accelerated methods rather than vanilla gradient-based method. Despite widely applied to arbitrary loss function, their behaviour in generically non-convex, high dimensional landscapes is poorly understood. In this work we used dynamical mean field theory techniques to describe analytically the average behaviour of these methods in a prototypical non-convex model: the (spiked) matrix-tensor model. We derive a closed set of equations that describe the behaviours of several algorithms including heavy-ball momentum and Nesterov acceleration. Additionally we characterize the evolution of a mathematically equivalent physical system of massive particles relaxing toward the bottom of an energetic landscape. Under the correct mapping the two dynamics are equivalent and it can be noticed that having a large mass increases the effective time step of the heavy ball dynamics leading to a speed up.

I. INTRODUCTION

In many computer science applications one of the critical steps is the minimization of a cost function. Apart from very few exceptions, the most simple way to approach the problem is by running local algorithms that move down in the cost landscape and hopefully approach a minimum at a small cost. The simplest algorithm of this kind is gradient descent, that has been used since the XIX century to address optimization problems [9] and it is still one of the most popular algorithms. Later on, faster and more stable algorithms have been developed, in particular second order methods [6, 19, 25, 29, 32, 47] where information from the Hessian are used to adapt the descent to the local geometry of the cost landscape, or first order methods based on momentum [2, 15, 31, 37, 38] that introduce inertia in the algorithm and provably speed-up convergence in a variety of convex problems. In the era of deep-learning and large datasets, the research has pushed towards memory efficient algorithms, in particular stochastic gradient descent that trades off computational and statistical efficiency [41, 50], and momentum-based methods are very used in practice [28]. Which algorithm is the best in practice seems not to have a simple answer and there are instances where a class of algorithms outperforms the other and vice-versa [26]. Most of the theoretical literature on momentum-based methods concerns convex problems [18, 23, 24, 30, 49] and, despite these methods have been successfully applied to a variety of problems, only recently high dimensional non-convex settings have been considered [22, 51, 52]. Furthermore, with few exceptions [45], the majority of these studies focus on *worst-case* analysis while empirically one could also be interested in the behaviour of such algorithms on

typical instances of the optimization problem, when this is extracted from a probability distribution.

The main result of this paper is the analytical description of the average evolution of momentum-based methods in two simple non-convex, high-dimensional, optimization problems. First we consider the mixed p -spin model [4, 21], a paradigmatic random high-dimensional optimization problem. Furthermore we consider its spiked version, the spiked matrix-tensor [40, 44] which is a prototype high-dimensional non-convex inference problem in which one wants to recover a signal hidden in the landscape.

The definition of the model and the algorithms used is reported in section II. In section III and IV we use dynamical mean field theory [11, 16, 33] to derive a set of equations that describes the average behaviour of these algorithms starting from random initialization in the high dimensional limit. To the best of our knowledge this is the first time that an analytic expression for the state evolution of accelerated gradient methods is derived in a high dimensional fully non-convex setting.

We apply our equations to the spiked matrix-tensor model which displays a similar phenomenology as the one described in [51] for the phase retrieval problem: all algorithms have two dynamical regimes. First, they navigate in the non-convex landscape and, second, if the signal to noise ratio is strong enough, the dynamics eventually enters in the basin of attraction of the signal and rapidly reaches the bottom of the cost function. We use the derived state evolution of the algorithms to determine their algorithmic threshold for signal recovery.

Furthermore we observe that using the best values of the setting parameters in the algorithms, momentum-based methods outperform vanilla gradient descent. Finally we show that in the analysed models, momentum-based methods only have an advantage in terms of speed but they do not outperform vanilla gradient in terms of algorithmic threshold. Indeed in section V we show that all the analysed methods share the same threshold.

* stefano.saraomannelli@psy.ox.ac.uk

† pierfrancesco.urbani@ipht.fr

II. MODEL DEFINITION

We consider two prototypical non-convex models: the mixed p -spin model [11, 13], and the spiked matrix-tensor model [40, 44]. Given a tensor in $(R^N)^{\otimes p}$ and a matrix in $\mathbb{R}^{N \times N}$, the goal is to find a common low-rank representation \mathbf{x} that minimizes the loss

$$\begin{aligned} \mathcal{L} = & -\frac{1}{\Delta_p} \sqrt{\frac{(p-1)!}{N^{p-1}}} \sum_{i_1, \dots, i_p=1}^N T_{i_1, \dots, i_p} x_{i_1} \dots x_{i_p} + \\ & -\frac{1}{\Delta_2} \frac{1}{\sqrt{N}} \sum_{i, j=1}^N Y_{ij} x_i x_j, \end{aligned} \quad (1)$$

with \mathbf{x} in the N -dimensional sphere of radius \sqrt{N} . The two problems differ by the definition of the variables \mathbf{T} and \mathbf{Y} . Call $\boldsymbol{\xi}^{(p)}$ and $\boldsymbol{\xi}^{(2)}$ and order p tensor and a matrix having i.i.d. Gaussian elements, with zero mean variance Δ_p and Δ_2 respectively. In the mixed p -spin model, tensor and matrix are completely random $\mathbf{T} = \boldsymbol{\xi}^{(p)}$ and $\mathbf{Y} = \boldsymbol{\xi}^{(2)}$. While in the spiked matrix-tensor model there is a low-rank representation given by $\mathbf{x}^* \in \mathbb{S}^{N-1}(\sqrt{N})$ embedded in the problem as follow:

$$T_{i_1 \dots i_p} = \sqrt{\frac{(p-1)!}{N^{p-1}}} x_{i_1}^* \dots x_{i_p}^* + \xi_{i_1 \dots i_p}^{(p)}, \quad (2)$$

$$Y_{ij} = \frac{x_i^* x_j^*}{\sqrt{N}} + \xi_{ij}^{(2)}. \quad (3)$$

These problems have been studied both in physics, computer science. In the physics literature, research has focused on the relationship of gradient descent and Langevin dynamics and the corresponding topology of the complex landscape [3, 10, 11, 13, 20, 21]. The state evolution of the gradient descent dynamics for the mixed spiked matrix-tensor model has been studied only more recently [43]. All this works considered simple gradient descent dynamics and its noisy (Langevin) dressing.

In this work we focus on accelerated methods and provide an analytical characterization of the average performance of these algorithms for the models introduced above. In order to simplify the analysis we relax the hard constraint on the norm of the vector \mathbf{x} and consider $\mathbf{x} \in \mathbb{R}^N$ while adding a penalty term to \mathcal{L} to enforce a soft constraint $\frac{\mu}{4N} (\sum_i x_i^2 - N)^2$, so that the total cost function is $\mathcal{H} = \mathcal{L} + \frac{\mu}{4N} (\sum_i x_i^2 - N)^2$. Using the techniques described in detail in the next section we write the state evolution for the following algorithms:

- **Nesterov acceleration** [37] starting from $\mathbf{y}[0] = \mathbf{x}[0] \in \mathbb{S}^{N-1}(\sqrt{N})$

$$x_i[t+1] = y_i[t] - \alpha \nabla \mathcal{H}(\mathbf{y}[t]), \quad (4)$$

$$y_i[t+1] = x_i[t+1] + \frac{t}{t+3} (x_i[t+1] - x_i[t]); \quad (5)$$

with α another control parameter.

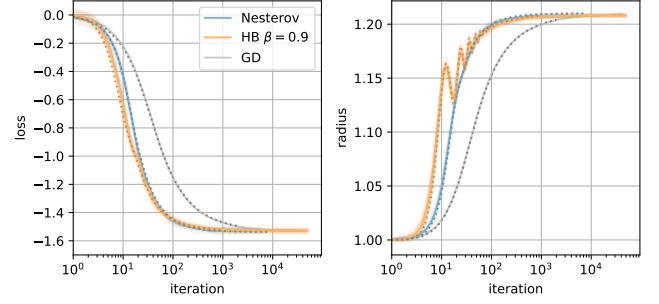


FIG. 1. **Simulation and DMFT comparison in mixed p -spin model.** The simulations in the figures have parameters with $p = 3$, $\Delta_3 = 2/p$, $\Delta_2 = 1$, ridge parameter $\mu = 10$ and input dimension $N = 1024$. In all our simulations we use the dilution technique [27, 46] to reduce the computational cost. We consider: Nesterov acceleration in blue; heavy ball momentum in orange with $\alpha = 0.01$ and $\beta = 0.9$; and gradient descent in grey. We run 100 simulations (in transparency) and draw the average. The parameters for heavy ball are the best parameters found in our simulations, see also Fig. 2 for a comparison. The results from the DMFT equations are drawn with dotted lines.

- **Polyak's or heavy ball momentum (HB)** [38] starting from $\mathbf{y}[0] = \mathbf{0}$ and $\mathbf{x}[0] \in \mathbb{S}^{N-1}(\sqrt{N})$

$$y_i[t+1] = \beta y_i[t] + \nabla \mathcal{H}(\mathbf{x}[t]), \quad (6)$$

$$x_i[t+1] = x_i[t] - \alpha y_i[t+1]; \quad (7)$$

with α and β two control parameters.

- **gradient descent (GD)** starting from $\mathbf{x}[0] \in \mathbb{S}^{N-1}(\sqrt{N})$

$$x_i[t+1] = x_i[t] - \alpha \nabla_i \mathcal{H}(\mathbf{x}[t]); \quad (8)$$

This case has been considered in [21, 43] in the case in which one enforces the constraint $\sum_i x_i^2 = N$. The generalization to the present case in which constraint is soft is a straightforward small extension of these previous works. However it will be used to benchmark the following two accelerated gradient methods.

We will not compare systematically the performance of these accelerated gradient methods to algorithms of different nature (such as for example message passing ones) in the same settings. Our goal will be the derivation of a set of dynamical equations describing the average evolution of such algorithms in the high dimensional limit $N \rightarrow \infty$.

III. DYNAMICAL MEAN FIELD THEORY

We use dynamical mean field theory (DMFT) techniques to derive sets of equation describing the evolution of the algorithms. The method has its origin in statistical

physics and can be applied to the study of Langevin dynamics of disordered systems [16, 33, 35]. More recently it was proved to be rigorous in the case of the mixed p -spin model [5, 17]. The application to the inference version of the optimization problem is in [43, 44]. The same techniques have also been applied to study the stochastic gradient descent dynamics in single layer networks [36] and in the analysis of recurrent neural networks [7, 34, 48]. The idea behind DMFT is that if the input dimension N is sufficiently large, one can obtain a description of the dynamics in terms of the typical evolution of a representative entry of the vector \mathbf{x} (and vector \mathbf{y} when applies). The representative element evolve according to a non-Markovian stochastic process whose memory term and noise source encode, in a self-consistent way, the interaction with all the other components of vector \mathbf{x} (and \mathbf{y}). The memory terms as well as the statistical properties of the noise are described by dynamical order parameters, which, in the present model are given by the dynamical two-time correlation and response functions.

In this first step of the analysis we therefore obtain an effective dynamics for a representative entry x_i (and y_i). The next step consists in using such equations to compute self-consistently the properties of the corresponding stochastic processes, namely the memory kernel and the statistical correlation of the noise. In Fig. 1 we anticipate the results by comparing numerical simulations with the integration of the DMFT equations for the different algorithms: on the left we observe the evolution of the loss, on the right we observe the evolution of the radius of the vector \mathbf{x} , defined as L_2 norm of the vector $\|\mathbf{x}\|_2$. We find a good agreement between the DMFT state evolution and the numerical simulations.

A. DMFT equations

In the following we describe the final DMFT equation for the correlation and response functions. The details of their derivation for the case of the Nesterov acceleration are provided in the following section, while we leave the other cases to the supporting information (SI). The dynamical order parameters appearing in the DMFT equations are one-time or two-time correlations, e.g. $C_{xy}[t, t'] = \sum_i x_i[t]y_i[t]/N$, and response to instantaneous perturbation of the dynamics, e.g. $R_x[t, t'] = (\sum_i \delta x_i[t]/\delta H_i[t'])/N$ by a local field \mathbf{H} . In this section we show only the equations for the mixed p -spin model and we discuss the difference and the derivation of the equations for the spiked tensor in the SI.

a. Nesterov acceleration. It has been shown that this algorithm has a quadratic convergence rate to the minimum in convex optimization problems thus it outperforms standard gradient descent whose convergence is linear in the number of iterations[37]. The analysis of the algorithm is described by the flow of the following dynamical

correlation functions

$$C_x[t, t'] = \sum_i x_i[t]x_i[t']/N, \quad (9)$$

$$C_y[t, t'] = \sum_i y_i[t]y_i[t']/N, \quad (10)$$

$$C_{xy}[t, t'] = \sum_i x_i[t]y_i[t]/N, \quad (11)$$

$$R_x[t, t'] = \frac{1}{N} \sum_i \frac{\delta x_i[t]}{\delta H_i[t']}, \quad (12)$$

$$R_y[t, t'] = \frac{1}{N} \sum_i \frac{\delta y_i[t]}{\delta H_i[t']}. \quad (13)$$

Following the procedure detailed in section IV we obtain the dynamical equations

$$\begin{aligned} C_x[t+1, t'] &= C_{xy}[t, t'] - \alpha\mu (C_y[t, t] - 1) C_y[t, t'] \\ &+ \alpha^2 \sum_{t''=0}^{t'} R_x[t', t''] Q'(C_y[t, t'']) + \\ &+ \alpha^2 \sum_{t''=0}^t R_y[t, t''] Q''(C_y[t, t'']) C_{xy}[t', t'']; \end{aligned} \quad (14)$$

$$\begin{aligned} C_{xy}[t+1, t'] &= C_y[t, t'] - \alpha\mu (C_y[t, t] - 1) C_{xy}[t, t'] \\ &+ \alpha^2 \sum_{t''=0}^{t'} R_y[t', t''] Q'(C_y[t, t'']) + \\ &+ \alpha^2 \sum_{t''=0}^t R_y[t, t''] Q''(C_y[t, t'']) C_y[t', t'']; \end{aligned} \quad (15)$$

$$C_{xy}[t', t+1] = \frac{2t+3}{t+3} C_x[t+1, t'] - \frac{t}{t+3} C_x[t, t']; \quad (16)$$

$$C_y[t', t+1] = \frac{2t+3}{t+3} C_{xy}[t+1, t'] - \frac{t}{t+3} C_{xy}[t, t']; \quad (17)$$

$$\begin{aligned} R_x[t+1, t'] &= R_y[t, t'] + \delta_{t, t'} \\ &- \alpha\mu (C_y[t, t] - 1) R_y[t, t'] \\ &+ \alpha^2 \sum_{t''=t'}^t R_y[t, t''] R_y[t'', t'] Q''(C_y[t, t'']); \end{aligned} \quad (18)$$

$$R_y[t', t+1] = \frac{2t+3}{t+3} R_x[t+1, t'] - \frac{t}{t+3} R_x[t, t']. \quad (19)$$

where $Q(x) = x^p/(p\Delta_p) + x^2/(2\Delta_2)$. The initial conditions are: $C_x[0, 0] = 1$, $C_y[0, 0] = 1$, $C_{xy}[0, 0] = 1$, $R_x[t+1, t] = 1$, $R_y[t+1, t] = \frac{2t+3}{t+3}$.

b. Heavy ball momentum. The simplest way to analyze the HB dynamics is by using the results of [39] to map it to the massive momentum described by the flow equation

$$m\ddot{x}_i(t) + \dot{x}_i(t) = -\frac{\delta \mathcal{H}[\mathbf{x}(t)]}{\delta x_i(t)}. \quad (20)$$

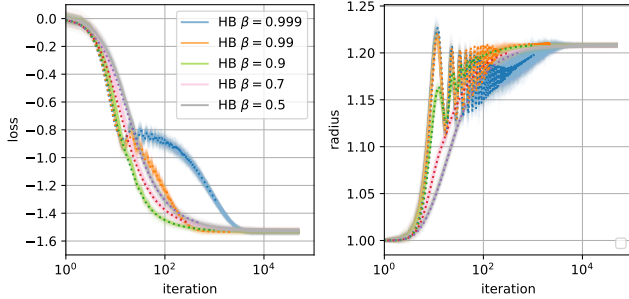


FIG. 2. Comparison of HB and massive with mapping. Simulations of HB momentum in the mixed p -spin model with $p = 3$, $\Delta_3 = 2/p$, $\Delta_2 = 1$, ridge parameter $\mu = 10$ and input dimension $N = 1024$. The parameters are $\alpha = 0.01$ for all the simulations and $\beta \in \{0.5, 0.7, 0.9, 0.99, 0.999\}$. We use solid line to represent the result from the simulation, the dotted line for the DMFT of massive gradient flow with the mapping. We observe that in this problem the value of β that gives the best speed up is $\beta = 0.9$. In order to integrate the DMFT of massive gradient we matched the mass as described in Eq. (22) and consider time steps $h \in \{0.005, 0.005, 0.0125, 0.25, 0.25\}$.

The natural discretization of this equation is

$$\begin{aligned} \frac{m}{h^2} (x[k+1] - 2x[k] - x[k-1]) + \frac{1}{h} (x[k+1] - x[k]) \\ = -\nabla \mathcal{L}(x[k]) \end{aligned} \quad (21)$$

being h the time discretization step (analogous to the learning rate in gradient descent). Using the mapping of [39] we can identify

$$m = \frac{\beta\alpha}{(1-\beta)^2} \quad (22)$$

$$h = \frac{\alpha}{1-\beta} \quad (23)$$

Observe that in order to be consistent with a continuous dynamics we need the following scaling $\beta = \mathcal{O}(1)$, $\alpha = \mathcal{O}[(1-\beta)^2]$. We empirically observe in the simulations a good agreement between massive and HB even for $\beta = 0.999$ and $\alpha = 0.01$. In the following, when discussing the comparison between simulation and DMFT, we mean that we run HB algorithm and superimpose on its massive momentum description.

The massive momentum dynamics was also considered in [14] without the damping term ($\dot{x}_i(t)$) and for the model with a hard spherical constraint $\sum_i x_i[t]^2 = N$. While the DMFT derived in [14] completely describe the aforementioned particular case, the way in which it is written uses the fact that without damping the dynamics is conservative and the spherical constraint can be enforced using that. In our case we are not in this regime and therefore we resort to a different computation, that will lead us to quite different equations. Indeed if one wants to transform massive momentum in a practical

algorithm one needs to transform the second order ODEs into first order by defining velocity variables $v_i(t) = \dot{x}_i(t)$. Then the discrete version of Eq. (20) is

$$\begin{aligned} x_i[t+1] &= x_i[t] + hv_i[t] \\ v_i[t+1] &= v_i[t] - \frac{h}{m} v_i[t] - \frac{h}{m} \frac{\delta \mathcal{H}}{\delta x_i[t]} \end{aligned} \quad (24)$$

Analysing these equations through DMFT one gets a set of flow equations for the following dynamical order parameters

$$C_x[t, t'] = \sum_i x_i[t] x_i[t'] / N, \quad (25)$$

$$C_v[t, t'] = \sum_i v_i[t] v_i[t'] / N, \quad (26)$$

$$C_{xv}[t, t'] = \sum_i x_i[t] v_i[t'] / N, \quad (27)$$

$$R_v[t, t'] = \frac{1}{N} \sum_i \frac{\delta v_i[t]}{\delta H_i[t']}, \quad (28)$$

$$R_{x|v}[t, t'] = \frac{1}{N} \sum_i \frac{\delta x_i[t]}{\delta H_i[t']}; \quad (29)$$

where \mathbf{H} is an instantaneous perturbation acting on the velocity. The result of the computation gives:

$$C_x[t+1, t'] = C_x[t, t'] + h C_{xv}(t', t); \quad (30)$$

$$\begin{aligned} C_v[t+1, t'] &= C_v[t, t'] - \frac{h}{m} C_v(t, t') \\ &\quad - \mu \frac{h}{m} C_{xv}(t, t') (C_x(t, t) - 1) \\ &\quad + \frac{h^2}{m} \sum_{t''=0}^t R_{x|v}[t, t''] Q''(C_x[t, t'']) C_{xv}[t'', t'] \end{aligned} \quad (31)$$

$$C_{xv}[t+1, t'] = C_{xv}[t, t'] + h C_v[t, t'] ; \quad (32)$$

$$\begin{aligned} C_{xv}[t, t'+1] &= C_{xv}[t, t'] - \frac{h}{m} C_{xv}[t, t'] \\ &\quad - \mu \frac{h}{m} C_x[t, t'] (C_x[t', t'] - 1) \\ &\quad + \frac{h^2}{m} \sum_{t''=0}^{t'} R_{x|v}[t', t''] Q''(C_x[t', t'']) C_x[t, t''] \\ &\quad + \frac{h^2}{m} \sum_{t''=0}^t Q'(C_x[t', t'']) R_{x|v}[t, t''] \end{aligned} \quad (33)$$

$$\begin{aligned} R_v[t+1, t'] &= R_v[t, t'] + \frac{h}{m} \delta_{t, t'} \\ &\quad - \mu \frac{h}{m} R_{x|v}[t, t'] (C_x(t, t) - 1) - \frac{h}{m} R_v[t, t'] \\ &\quad + \frac{h^2}{m} \sum_{t''=0}^t Q''(C_x[t, t'']) R_{x|v}[t, t''] R_{x|v}[t'', t'] \end{aligned} \quad (34)$$

$$R_{x|v}[t+1, t'] = R_{x|v}[t, t'] + h R_v[t, t']. \quad (35)$$

and initial conditions : $C_x[0, 0] = 1$, $C_v[0, 0] = 0$, $C_{xv}[0, 0] = 0$, $R_v[t+1, t] = 1/m$, $R_{x|v}[t+1, t] = 0$.

c. *Gradient descent.* A simple way to obtain the gradient descent DMFT is by taking the limit $m \rightarrow 0$ in the DMFT of the massive momentum description of HB. We get

$$\begin{aligned} C_x[t+1, t'] &= C_x[t, t'] - \alpha\mu (C_x[t, t] - 1) C_x[t, t'] \\ &+ \alpha^2 \sum_{t''=0}^{t'} R_x[t', t''] Q' (C_x[t, t'']) \\ &+ \alpha^2 \sum_{t''=0}^t R_x[t, t''] Q'' (C_x[t, t'']) C_x[t', t'']; \\ R_x[t+1, t'] &= R_x[t, t'] + \delta_{t, t'} \\ &- \alpha\mu (C_x[t, t] - 1) R_x[t, t'] \\ &+ \alpha^2 \sum_{t''=0}^t R_x[t, t''] R_x[t'', t'] Q'' (C_x[t, t'']). \end{aligned} \quad (36) \quad (37)$$

with initial conditions: $C_x[0, 0] = 1$, and $R_x[t+1, t] = 1$. Apart from the μ -dependent term, these equations are a particular case of the ones that appear in [12, 13] and we will point to these previous references for details.

d. *Observables.* From the order parameters obtained using the DMFT we can evaluate useful quantities that describe the evolution of the algorithms. In particular in Figs. 1,2,3 we show the loss, the radius (and the overlap with the solution for what concerns Fig. 3). The dynamical evolution of the average loss along the dynamics is given by

$$\begin{aligned} \mathcal{L}[t] &= -\frac{\alpha}{\Delta_p} \sum_{t''=0}^t R_x[t, t'] C_x[t, t']^{p-1} / C_x[t, t]^{\frac{p}{2}} \\ &- \frac{\alpha}{\Delta_2} \sum_{t''=0}^t R_x[t, t'] C_x[t, t'] / C_x[t, t] \end{aligned} \quad (38)$$

The radius is simply given by $\sqrt{C_x[t, t]}$. While the overlap with the solution in the spiked case is given by $\frac{\mathbf{x}[t] \cdot \mathbf{x}^*}{\sqrt{\|\mathbf{x}\|}} = m_x[t] / \sqrt{C_x[t, t]}$ by definition, where $m_x[t] = \frac{1}{N} \sum_i x_i[t] x_i^*$ is an additional order parameter required in the spiked matrix tensor model as described in the SI.

We compare Nesterov acceleration with the heavy ball momentum as described by the mapping to Massive momentum in Fig. 1 for the mixed p -spin model, and in Fig. 3 for the spiked model. Nesterov acceleration allows a fast convergence to the asymptotic energy without need of parameter tuning. In Fig. 2 we instead compare the numerical simulations for the HB algorithm and the DMFT description of the corresponding massive momentum version for several control parameters.

IV. DMFT FOR NESTEROV ACCELERATION

We use the dynamical cavity method [35] to derive the equations. We start by looking at the gradient of the total cost function $\nabla \mathcal{H} = \sum_j J_{ij} x_j + \sum_{i_1, \dots, i_p} J_{i_1, \dots, i_p} x_{i_1} \dots x_{i_p} + \frac{\mu}{N} \left(\sum_{j=1}^N x_j^2 - N \right) x_i$. We consider the problem having in dimension $N+1$ and we denote the additional entry of the vectors \mathbf{x} and \mathbf{y} as the component x_0 and y_0 . The idea behind DMFT is to track how this additional degrees of freedom changes the dynamics of all degrees of freedom. If the dimension is sufficiently high (N large) the dynamics is not largely modified by the additional dimension, and the effect of the additional degree of freedom can be tracked in perturbation theory. Therefore we consider the Nesterov update algorithm and isolate the effect of the additional degree of freedom. We have

$$x_i[t+1] = y_i[t] + \alpha \sum_{j \neq 0} J_{ij} y_j[t] \quad (39)$$

$$+ \alpha \sum_{(i, i_2, \dots, i_p)} J_{i, i_2, \dots, i_p} y_{i_2}[t] \dots y_{i_p}[t] \quad (40)$$

$$- \alpha\mu \left(\sum_{j \neq 0} y_j^2[t]/N - 1 \right) y_i[t] \quad (41)$$

$$+ \alpha \sum_{(i, i_3, \dots, i_p)} J_{i, 0, i_3, \dots, i_p} y_0[t] y_{i_3}[t] \dots y_{i_p}[t] \quad (42)$$

$$+ \alpha J_{i0} y_0[t] + \frac{\mu}{N} y_0^2[t] y_i[t], \quad (43)$$

$$y_i[t+1] = x_i[t+1] + \frac{t}{t+3} (x_i[t+1] - x_i[t]), \quad (44)$$

identify lines (42,43) with the perturbation acting on the dynamics $H_i[t]$. In the linear response regime, the perturbed spin are given by:

$$x_i[t] \approx x_i^0 + \alpha \sum_{t''=0}^t \frac{\delta x_i[t]}{\delta H_i[t'']} H_i[t''], \quad (45)$$

$$y_i[t] \approx y_i^0 + \alpha \sum_{t''=0}^t \frac{\delta y_i[t]}{\delta H_i[t'']} H_i[t'']. \quad (46)$$

Therefore the dynamics of the 0th position to the leading order in the perturbation is

$$x_0[t+1] = y_0[t] - \alpha\mu \left(\sum_j y_j^2[t]/N - 1 \right) y_0[t] \quad (47)$$

$$+ \overbrace{\alpha \sum_j J_{0j} y_j[t] + \alpha \sum_{(0, i_2, \dots, i_p)} J_{0, i_2, \dots, i_p} y_{i_2}[t] \dots y_{i_p}[t]}^{\doteq \Xi[t]} \quad (48)$$

$$+ \alpha^2 \sum_j J_{0j} \sum_{t''=0}^t \frac{\delta y_j[t]}{\delta H_j[t'']} H_j[t''] \quad (49)$$

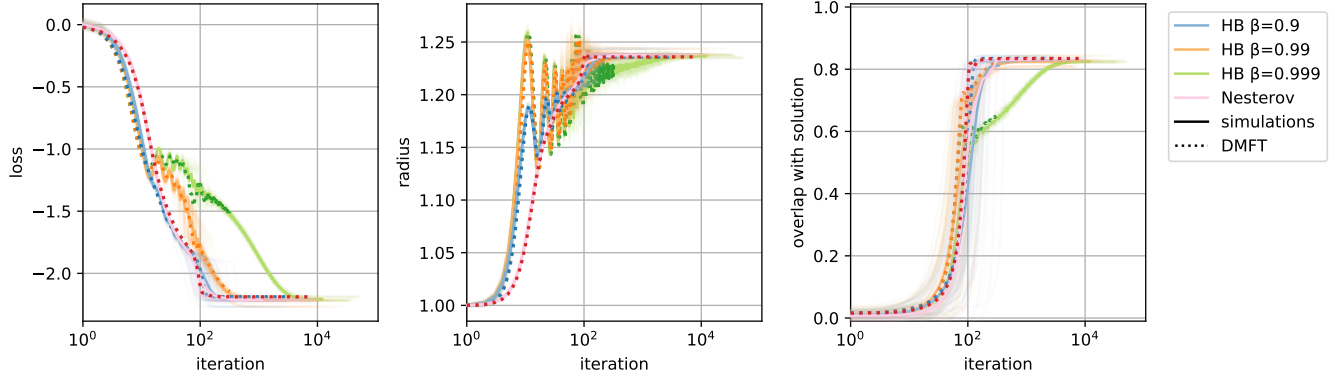


FIG. 3. **DMFT in the spiked matrix-tensor model.** Performance of heavy ball and Nesterov in the spiked matrix-tensor model with $p = 3$, $1/\Delta_2 = 2.7$, $\Delta_3 = 1.0$, and $\mu = 10$. For heavy ball we used the following parameters: α is kept fixed to 0.01 and $\beta = 0.9, 0.99, 0.999$. The different solid lines correspond to different input dimension, while the dotted line is obtained from the DMFT that by definition is in infinite dimension limit. For heavy ball we used the DMFT of massive momentum with time steps $h = 0.01, 0.01, 0.1$ (respectively) and mass given by Eq. (22). We can see that in the spiked model the finite size effects are stronger and we need larger simulation sizes to find a better agreement with the theory.

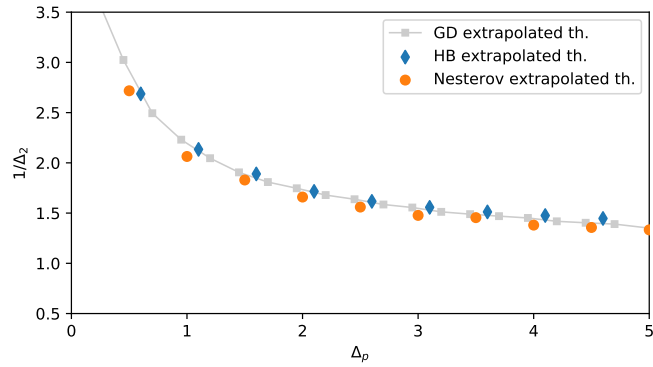


FIG. 4. **Phase diagram of the spiked matrix-tensor model.** The horizontal and vertical axis represent the parameters of the model Δ_p and $1/\Delta_2$. We identify two regions in the diagram: where Nesterov, heavy ball and gradient descent algorithms lead to the hidden solution (upper region), and where it does not (lower region). The grey square connected by a solid line represents the threshold of gradient descent estimated numerically as detailed in the text. We use points to indicate the threshold extrapolated from the DMFT: blue circles for Nesterov acceleration and orange diamonds for heavy ball momentum with $\beta = 0.5$ and $\alpha = 0.01$. In the mapping with massive momentum we consider the mass and time steps obtained from Eqs. (22,23).

$$+ \alpha^2 \sum_{(0,i_2,\dots,i_p)} J_{0,i_2,\dots,i_p} \left(\sum_{t''=0}^t \frac{\delta y_{i_2}[t]}{\delta H_{i_2}[t'']} \times \right. \quad (50)$$

$$\left. \times H_{i_2}[t''] y_{i_2}[t] \dots y_{i_p}[t] + \text{perm.} \right) \quad (51)$$

$$- \frac{2\alpha\mu}{N} \sum_j \sum_{t''=0}^t \frac{\delta y_j[t]}{\delta H_j[t'']} H_j[t''] y_j[t] y_0[t], \quad (52)$$

$$y_i[t+1] = x_i[t+1] + \frac{t}{t+3} (x_i[t+1] - x_i[t]). \quad (53)$$

We defined Ξ a Gaussian stochastic process with moments: $\mathbb{E}[\Xi[t]] = 0$, and $\mathbb{E}[\Xi[t]\Xi[t']] = \frac{1}{\Delta_2} C_y[t,t'] + \frac{1}{\Delta_p} C_y^{p-1}[t,t'] = Q'(C_y[t,t']) \doteq \mathbb{K}[t,t']$. We can now move towards lines (49-52) and work on simplifying these equa-

tions. We start with line (49):

$$\alpha^2 \sum_j J_{0j} \sum_{t''=0}^t \frac{\delta y_j[t]}{\delta H_j[t'']} J_{0j} y_0[t''] \quad (54)$$

$$\approx \frac{\alpha^2}{\Delta_2 N} \sum_{t''=0}^t \frac{\delta y_j[t]}{\delta H_j[t'']} y_0[t''] \quad (55)$$

$$= \frac{\alpha^2}{\Delta_2} \sum_{t''=0}^t R_y[t,t''] y_0[t'']. \quad (56)$$

Where line (56) follows by the definition of response function in y . Moving towards lines (50,51), and carefully

taking into account the permutations, we obtain

$$\frac{\alpha^2(p-1)}{\Delta_p} \sum_{t''=0}^t R_y[t, t''] (C_y[t, t''])^{p-2} y_0[t'']. \quad (57)$$

Finally we can easily see that the term deriving from the regulariser is subleading in N .

Therefore we finally obtain that the additional degree of freedom obeys the effective dynamics

$$x_0[t+1] = y_0[t] + \alpha \Xi[t] - \alpha \mu (C_y[t, t] - 1) y_0[t] + \alpha^2 \sum_{t''=0}^t R_y[t, t''] Q'' (C_y[t, t'']) y_0[t'']; \quad (58)$$

$$y_0[t+1] = x_0[t+1] + \frac{t}{t+3} (x_0[t+1] - x_0[t]). \quad (59)$$

We need to evaluated the expected values of $\langle \Xi[t] x_0[t'] \rangle$ and $\langle \Xi[t] y_0[t'] \rangle$ with respect to the stochastic process. Given Ξ , we use the Girsanov theorem to get

$$\begin{aligned} \langle \Xi[t] x_0[t'] \rangle &= \alpha \sum_{t''} R_x[t', t''] Q' (C_y[t, t'']), \\ \langle \Xi[t] y_0[t'] \rangle &= \alpha \sum_{t''} R_y[t', t''] Q' (C_y[t, t'']). \end{aligned} \quad (60)$$

Final step consists in substituting the Eqs. (58,59) into the equations of the order parameters Eqs. (14–19). Then we identify the order parameters in the equations and use the results of Girsanov theorem to obtain the dynamical equations reported in section III.

V. ALGORITHMIC THRESHOLD

In this section we consider the generalization of the accelerated methods to investigate how they perform the task of recovering a signal in a complex non-convex landscape. We therefore focus on the spiked matrix-tensor model. In [43], using DMFT, the dynamics of the gradient descent algorithm was analyzed and the phase diagram for signal recovery was characterized in terms of the noise levels Δ_2 and Δ_3 . At fixed Δ_3 , one has that is Δ_2 is small enough, the gradient descent algorithm manages to get very close to the signal, while if it is too low, the overlap of the estimator with the true signal stays at zero while the gradient descent dynamics descend the landscape towards uninformative local minima.

In this section we redo for the accelerated gradient methods the same numerical analysis proposed in [43] whose results were confirmed theoretically in [42]. We fix the order of the tensor to be $p = 3$. We again expect that at fixed Δ_3 , increasing Δ_2 one goes from an easy phase where the signal can be partially recovered, to an algorithmically impossible phase where instead the final overlap with the signal vanishes. Therefore we are interested in characterizing the corresponding algorithmic threshold. In order to do that we follow [43] and approach

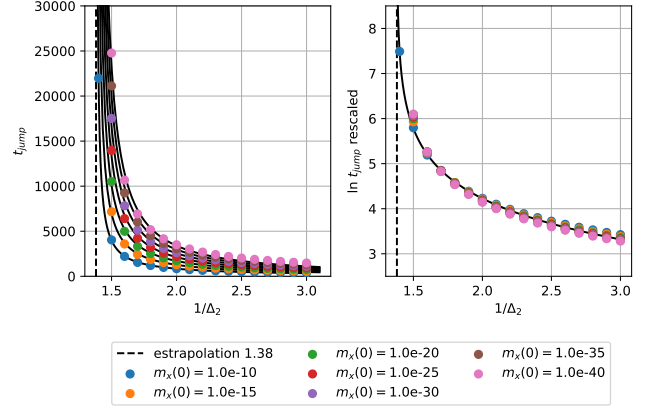


FIG. 5. **Algorithmic threshold extrapolated using Nesterov acceleration.** The dots are the divergence time obtained for the different values of Δ_2 with $\Delta_3 = 4.0$ fixed. The threshold obtained by fitting with a power law and observing the divergent Δ_2 . The result gives $1/\Delta_2 = 1.38$ that is very close to the analytical value $1/\Delta_2 = 1.37$ for gradient descent. On the left panel we plot the number of iteration before the algorithm jumps to the solution t_{jump} as a function of the signal to noise ratio $1/\Delta_2$. The figure also show remarkable finite size effects for different initial conditions of m_x and m_y . The same kind of finite size effects where also observed in [43]. On the right panel we show that these lines collapse to a single line once rescaled by a factor $a^{\ln m_x[0]}$ with $a \approx 1.089$.

the transition line from the easy phase and measure, using the DMFT, the relaxation time of the accelerated methods towards the signal. This time diverges on approaching the algorithmic threshold and by fitting the corresponding divergence we estimate the boundary between the easy and algorithmically impossible phase.

For a fixed value of Δ_3 , as we increase the noise to signal ratio (Δ_2 increases) the simulation time required to close to the signal increases like a power law $\sim a |\Delta_2 - \Delta_2^{al}(\Delta_3)|^{-\theta}$. The algorithmic threshold $\Delta_2^{al}(\Delta_3)$ is obtained by fitting the parameters of the power law $(a, \theta, \Delta_2^{al})$. The extrapolation procedure is shown in Fig. 5 for $\Delta_3 = 4.0$. We consider many different initial conditions $m_x(0)$ in order to correctly characterize the limits as $N \rightarrow \infty$ and $m_x(0) \rightarrow 0^+$. Finally the fits obtained for the three algorithms and for several Δ_3 are shown in the phase diagram of Fig. 4. We find that all algorithms give comparable threshold for partial signal recovery.

VI. CONCLUSIONS AND PERSPECTIVES

In this work we analysed momentum-accelerated methods in two paradigmatic high-dimensional non-convex problems: the mixed p -spin model and the spiked matrix-tensor model. Our analysis is based on dynamical mean field theory and provides a set of equations that correctly

characterize the average evolution of the dynamics. We have focused on Polyak's heavy ball and Nesterov acceleration, but the same techniques apply as well to more recent methods such as quasi-hyperbolic momentum [31] and proportional integral-derivative control algorithm [2]. The computations can be also extended to discuss how accelerated training algorithms perform in other models such as 1-layer feedforward networks [36], and recurrent networks [7, 34].

VII. ACKNOWLEDGEMENTS

The authors thank Andrew Saxe for precious discussions. This work was supported by the Wellcome Trust and Royal Society (grant number 216386/Z/19/Z), and by "Investissements d'Avenir" LabEx-PALM (ANR-10-LABX-0039-PALM).

[1] Agoritsas, E., Biroli, G., Urbani, P., and Zamponi, F. Out-of-equilibrium dynamical mean-field equations for the perceptron model. *Journal of Physics A: Mathematical and Theoretical*, 51(8):085002, 2018.

[2] An, W., Wang, H., Sun, Q., Xu, J., Dai, Q., and Zhang, L. A pid controller approach for stochastic optimization of deep networks. In *Proceedings of the IEEE Conference on Computer Vision and Pattern Recognition*, pp. 8522–8531, 2018.

[3] Auffinger, A., Ben Arous, G., and Černý, J. Random matrices and complexity of spin glasses. *Communications on Pure and Applied Mathematics*, 66(2):165–201, 2013.

[4] Barrat, A., Franz, S., and Parisi, G. Temperature evolution and bifurcations of metastable states in mean-field spin glasses, with connections with structural glasses. *Journal of Physics A: Mathematical and General*, 30(16):5593–5612, aug 1997. doi:10.1088/0305-4470/30/16/006. URL <https://doi.org/10.1088/0305-4470/30/16/006>.

[5] Ben Arous, G., Dembo, A., and Guionnet, A. Cugliandolo-Kurchan equations for dynamics of spin-glasses. *Probability theory and related fields*, 136(4):619–660, 2006.

[6] Broyden, C. G. The convergence of a class of double-rank minimization algorithms: 2. the new algorithm. *IMA journal of applied mathematics*, 6(3):222–231, 1970.

[7] Can, T., Krishnamurthy, K., and Schwab, D. J. Gating creates slow modes and controls phase-space complexity in grus and lstms. In *Mathematical and Scientific Machine Learning*, pp. 476–511. PMLR, 2020.

[8] Castellani, T. and Cavagna, A. Spin-glass theory for pedestrians. *Journal of Statistical Mechanics: Theory and Experiment*, 2005(05):P05012, 2005.

[9] Cauchy, A. et al. Méthode générale pour la résolution des systèmes d'équations simultanées. *Comp. Rend. Sci. Paris*, 25(1847):536–538, 1847.

[10] Crisanti, A. and Leuzzi, L. Spherical 2+ p spin-glass model: An analytically solvable model with a glass-to-glass transition. *Physical Review B*, 73(1):014412, 2006.

[11] Crisanti, A. and Sommers, H.-J. The spherical-spin interaction spin glass model: the statics. *Zeitschrift für Physik B Condensed Matter*, 87(3):341–354, 1992.

[12] Crisanti, A., Horner, H., and Sommers, H.-J. The spherical-spin interaction spin-glass model. *Zeitschrift für Physik B Condensed Matter*, 92(2):257–271, 1993.

[13] Cugliandolo, L. F. and Kurchan, J. Analytical solution of the off-equilibrium dynamics of a long-range spin-glass model. *Physical Review Letters*, 71(1):173, 1993.

[14] Cugliandolo, L. F., Lozano, G. S., and Nesi, E. N. Non equilibrium dynamics of isolated disordered systems: the classical hamiltonian p-spin model. *Journal of Statistical Mechanics: Theory and Experiment*, 2017(8):083301, 2017.

[15] Cyrus, S., Hu, B., Van Scy, B., and Lessard, L. A robust accelerated optimization algorithm for strongly convex functions. In *2018 Annual American Control Conference (ACC)*, pp. 1376–1381. IEEE, 2018.

[16] De Dominicis, C. Dynamics as a substitute for replicas in systems with quenched random impurities. *Physical Review B*, 18(9):4913, 1978.

[17] Dembo, A. and Subag, E. Dynamics for spherical spin glasses: disorder dependent initial conditions. *Journal of Statistical Physics*, pp. 1–50, 2020.

[18] Flammarion, N. and Bach, F. From averaging to acceleration, there is only a step-size. In *Conference on Learning Theory*, pp. 658–695. PMLR, 2015.

[19] Fletcher, R. A new approach to variable metric algorithms. *The computer journal*, 13(3):317–322, 1970.

[20] Folena, G., Franz, S., and Ricci-Tersenghi, F. Gradient descent dynamics in the mixed p-spin spherical model: finite size simulation and comparison with mean-field integration. *arXiv preprint arXiv:2007.07776*, 2020.

[21] Folena, G., Franz, S., and Ricci-Tersenghi, F. Rethinking mean-field glassy dynamics and its relation with the energy landscape: The surprising case of the spherical mixed p-spin model. *Physical Review X*, 10(3):031045, 2020.

[22] Gadat, S., Panloup, F., Saadane, S., et al. Stochastic heavy ball. *Electronic Journal of Statistics*, 12(1):461–529, 2018.

[23] Ghadimi, E., Feyzmahdavian, H. R., and Johansson, M. Global convergence of the heavy-ball method for convex optimization. In *2015 European control conference (ECC)*, pp. 310–315. IEEE, 2015.

[24] Gitman, I., Lang, H., Zhang, P., and Xiao, L. Understanding the role of momentum in stochastic gradient methods. In Wallach, H., Larochelle, H., Beygelzimer, A., d'Alché-Buc, F., Fox, E., and Garnett, R. (eds.), *Advances in Neural Information Processing Systems*, volume 32, pp. 9633–9643. Curran Associates, Inc., 2019. URL <https://proceedings.neurips.cc/paper/2019/file/4eff0720836a198b6174eeccf02cbfdbf-Paper.pdf>.

[25] Goldfarb, D. A family of variable-metric methods derived by variational means. *Mathematics of computation*, 24(109):23–26, 1970.

[26] Kidambi, R., Netrapalli, P., Jain, P., and Kakade, S. On the insufficiency of existing momentum schemes for stochastic optimization. In *2018 Information Theory and Applications Workshop (ITA)*, pp. 1–9. IEEE, 2018.

[27] Krzakala, F. and Zdeborová, L. Performance of simulated annealing in p-spin glasses. In *Journal of Physics: Conference Series*, volume 473, pp. 012022. IOP Publishing,

2013.

[28] Lessard, L., Recht, B., and Packard, A. Analysis and design of optimization algorithms via integral quadratic constraints. *SIAM Journal on Optimization*, 26(1):57–95, 2016.

[29] Levenberg, K. A method for the solution of certain nonlinear problems in least squares. *Quarterly of applied mathematics*, 2(2):164–168, 1944.

[30] Loizou, N. and Richtárik, P. Momentum and stochastic momentum for stochastic gradient, newton, proximal point and subspace descent methods. *Computational Optimization and Applications*, 77(3):653–710, 2020.

[31] Ma, J. and Yarats, D. Quasi-hyperbolic momentum and adam for deep learning. In *7th International Conference on Learning Representations, ICLR 2019, New Orleans, LA, USA, May 6-9, 2019*. OpenReview.net, 2019. URL <https://openreview.net/forum?id=S1fUpoR5FQ>.

[32] Marquardt, D. W. An algorithm for least-squares estimation of nonlinear parameters. *Journal of the society for Industrial and Applied Mathematics*, 11(2):431–441, 1963.

[33] Martin, P. C., Siggia, E., and Rose, H. Statistical dynamics of classical systems. *Physical Review A*, 8(1):423, 1973.

[34] Mastrogiuseppe, F. and Ostojic, S. Intrinsically-generated fluctuating activity in excitatory-inhibitory networks. *PLoS computational biology*, 13(4):e1005498, 2017.

[35] Mézard, M., Parisi, G., and Virasoro, M. A. *Spin glass theory and beyond: An Introduction to the Replica Method and Its Applications*, volume 9. World Scientific Publishing Company, 1987.

[36] Mignacco, F., Krzakala, F., Urbani, P., and Zdeborová, L. Dynamical mean-field theory for stochastic gradient descent in gaussian mixture classification. In *2020 Conference on Neural Information Processing Systems-NeurIPS 2020*, 2020.

[37] Nesterov, Y. E. A method for solving the convex programming problem with convergence rate $o(1/k^2)$. In *Dokl. akad. nauk Sssr*, volume 269, pp. 543–547, 1983.

[38] Polyak, B. T. Some methods of speeding up the convergence of iteration methods. *USSR Computational Mathematics and Mathematical Physics*, 4(5):1–17, 1964.

[39] Qian, N. On the momentum term in gradient descent learning algorithms. *Neural networks*, 12(1):145–151, 1999.

[40] Richard, E. and Montanari, A. A statistical model for tensor pca. In Ghahramani, Z., Welling, M., Cortes, C., Lawrence, N., and Weinberger, K. Q. (eds.), *Advances in Neural Information Processing Systems*, volume 27, pp. 2897–2905. Curran Associates, Inc., 2014. URL <https://proceedings.neurips.cc/paper/2014/file/b5488aeff42889188d03c9895255cecc-Paper.pdf>.

[41] Robbins, H. and Monroe, S. A stochastic approximation method. *The annals of mathematical statistics*, pp. 400–407, 1951.

[42] Sarao Mannelli, S., Biroli, G., Cammarota, C., Krzakala, F., and Zdeborová, L. Who is afraid of big bad minima? analysis of gradient-flow in spiked matrix-tensor models. In *Advances in Neural Information Processing Systems*, pp. 8679–8689, 2019.

[43] Sarao Mannelli, S., Krzakala, F., Urbani, P., and Zdeborová, L. Passed & spurious: Descent algorithms and local minima in spiked matrix-tensor models. In *International Conference on Machine Learning*, pp. 4333–4342, 2019.

[44] Sarao Mannelli, S., Biroli, G., Cammarota, C., Krzakala, F., Urbani, P., and Zdeborová, L. Marvels and pitfalls of the langevin algorithm in noisy high-dimensional inference. *Physical Review X*, 10(1):011057, 2020.

[45] Scieur, D. and Pedregosa, F. Universal average-case optimality of polyak momentum. In III, H. D. and Singh, A. (eds.), *Proceedings of the 37th International Conference on Machine Learning*, volume 119 of *Proceedings of Machine Learning Research*, pp. 8565–8572. PMLR, 13–18 Jul 2020. URL <http://proceedings.mlr.press/v119/scieur20a.html>.

[46] Semerjian, G., Cugliandolo, L. F., and Montanari, A. On the stochastic dynamics of disordered spin models. *Journal of statistical physics*, 115(1):493–530, 2004.

[47] Shanno, D. F. Conditioning of quasi-newton methods for function minimization. *Mathematics of computation*, 24(111):647–656, 1970.

[48] Sompolinsky, H., Crisanti, A., and Sommers, H.-J. Chaos in random neural networks. *Physical review letters*, 61(3): 259, 1988.

[49] Sun, T., Yin, P., Li, D., Huang, C., Guan, L., and Jiang, H. Non-ergodic convergence analysis of heavy-ball algorithms. In *Proceedings of the AAAI Conference on Artificial Intelligence*, volume 33, pp. 5033–5040, 2019.

[50] Sutskever, I., Martens, J., Dahl, G., and Hinton, G. On the importance of initialization and momentum in deep learning. In *International conference on machine learning*, pp. 1139–1147. PMLR, 2013.

[51] Wang, J.-K. and Abernethy, J. Quickly finding a benign region via heavy ball momentum in non-convex optimization. *arXiv preprint arXiv:2010.01449*, 2020.

[52] Yang, T., Lin, Q., and Li, Z. Unified convergence analysis of stochastic momentum methods for convex and non-convex optimization. *arXiv preprint arXiv:1604.03257*, 2016.

Appendix A: Derivation of the DMFT equations for massive gradient flow

In this section we derive the dynamical mean field theory (DMFT) equations of massive gradient flow in the mixed p -spin.

We use the generating functional approach described in [1, 8] to obtain the effective dynamical equations. First we rewrite de massive dynamics Eq. (20) as two ODEs

$$m\dot{\mathbf{v}}(t) = -\mathbf{v}(t) - \nabla \mathcal{H}[\mathbf{x}(t)], \quad (\text{A1})$$

$$\dot{\mathbf{x}}(t) = \mathbf{v}(t). \quad (\text{A2})$$

We use the following simple identity that takes the name of *generating functional*

$$1 = \mathcal{Z} = \int \mathcal{D}[\mathbf{x}, \mathbf{v}] \delta(m\dot{\mathbf{v}}(t) + \mathbf{v}(t) + \nabla \mathcal{H}[\mathbf{x}(t)]) \delta(\dot{\mathbf{x}}(t) - \mathbf{v}(t)) \quad (\text{A3})$$

$$= \int \mathcal{D}[\mathbf{x}, \tilde{\mathbf{x}}, \mathbf{v}, \tilde{\mathbf{v}}] \prod_{i=1}^N \exp \left\{ i \int \tilde{v}_i(t) [m\dot{v}_i(t) + v_i(t) + \nabla_i \mathcal{H}[\mathbf{x}(t)]] dt \right\} \exp \left\{ i \int \tilde{x}_i(t) [\dot{x}_i(t) - v_i(t)] dt \right\} \quad (\text{A4})$$

where in the first line we integrate over all possible trajectories of \mathbf{v} and \mathbf{x} , and we impose them to match the massive gradient flow equations using Dirac's deltas. In the second line we use the Fourier representation of the delta and we absorb the normalization constants in the term $\mathcal{D}[\mathbf{x}, \tilde{\mathbf{x}}, \mathbf{v}, \tilde{\mathbf{v}}]$. We can now average over the stochasticity of the problem, let us indicate with an overline the average.

$$1 = \overline{\mathcal{Z}} = \int \mathcal{D}[\mathbf{x}, \tilde{\mathbf{x}}, \mathbf{v}, \tilde{\mathbf{v}}] \prod_{i=1}^N \exp \left\{ i \int \tilde{v}_i(t) [m\dot{v}_i(t) + v_i(t)] dt \right\} \exp \left\{ i \int \tilde{x}_i(t) [\dot{x}_i(t) - v_i(t)] dt \right\} \times \quad (\text{A5})$$

$$\times \overline{\prod_{i=1}^N \exp \left\{ i \int \tilde{v}_i(t) \left[\sqrt{\frac{(p-1)!}{N^{p-1}}} \sum_{(i, i_2, \dots, i_p)} \xi_{i, i_2, \dots, i_p}^{(p)} x_{i_2}(t) \dots x_{i_p}(t) + \frac{1}{\sqrt{N}} \sum_j \xi_{i, j}^{(2)} x_j(t) \right] dt \right\}} \times \quad (\text{A6})$$

$$\times \prod_{i=1}^N \exp \left\{ i \int \tilde{v}_i(t) \mu \left(\frac{1}{N} \sum_j x_j^2(t) - 1 \right) x_i(t) dt \right\} \quad (\text{A7})$$

We can proceed integrating the second line over the noise. Importantly we must group all the element that multiply a given $\xi^{(p)}$. Considering only second line and neglecting constant multiplicative factors we obtain

$$\begin{aligned} & \exp \left\{ -\frac{N}{2p\Delta_p} \int \left[p \left(\frac{1}{N} \sum_i \tilde{v}_i(t) \tilde{v}_i(t') \right) \left(\frac{1}{N} \sum_i x_i(t) x_i(t') \right)^{p-1} + \right. \right. \\ & \quad \left. \left. + p(p-1) \left(\frac{1}{N} \sum_i \tilde{v}_i(t) x_i(t') \right) \left(\frac{1}{N} \sum_i x_i(t) \tilde{v}_i(t') \right) \left(\frac{1}{N} \sum_i x_i(t) x_i(t') \right)^{p-2} \right] dt' dt \right\} \times \\ & \times \exp \left\{ -\frac{N}{2\Delta_2} \int \left[\left(\frac{1}{N} \sum_i \tilde{v}_i(t) \tilde{v}_i(t') \right) \left(\frac{1}{N} \sum_i x_i(t) x_i(t') \right) + \left(\frac{1}{N} \sum_i \tilde{v}_i(t) x_i(t') \right) \left(\frac{1}{N} \sum_i x_i(t) \tilde{v}_i(t') \right) \right] dt' dt \right\} \end{aligned}$$

We define $Q(x) = x^p/(p\Delta_p) + x^2/(2\Delta_2)$ Next we introduce some order parameters that are enforced using Dirac's deltas

$$\begin{aligned} & \int \mathcal{D}[C_x, C_{\tilde{v}}, C_{x\tilde{v}}, C_{\tilde{v}x}] \delta \left(NC_{\tilde{v}}(t, t') - \sum_j i \tilde{v}_j(t) i \tilde{v}_j(t') \right) \delta \left(NC_x(t, t') - \sum_j x_j(t) x_j(t') \right) \times \\ & \times \delta \left(NC_{x\tilde{v}}(t, t') - \sum_j x_j(t) i \tilde{v}_j(t') \right) \delta \left(NC_{\tilde{v}x}(t, t') - \sum_j i \tilde{v}_j(t) x_j(t') \right) \times \\ & \times \exp \left\{ -\frac{N}{2\Delta_p} \int \left[C_{\tilde{v}}(t, t') Q' [C_x(t, t')] + C_{\tilde{v}x}(t, t') C_{x\tilde{v}}(t, t') Q'' [C_x(t, t')] \right] dt' dt \right\}. \end{aligned}$$

Using again the Fourier representation of the deltas and considering N large, the auxiliary variables introduced with the transform concentrate to their saddle point according to Laplace approximation. Furthermore it is easy to show [8] that $C_{x\tilde{v}}(t, t') = C_{\tilde{v}x}(t', t)$ and $C_{x\tilde{v}}(t, t') = R_{x|v}(t, t')$, with $R_{x|v}$ defined in Eq. (29). Under this considerations, we rewrite the average generating functional

$$1 = \bar{\mathcal{Z}} = \int \mathcal{D}[\mathbf{x}, \tilde{\mathbf{x}}, \mathbf{v}, \tilde{\mathbf{v}}] \prod_{i=1}^N \exp \left\{ i \int \tilde{v}_i(t) \left[m\dot{v}_i(t) + v_i(t) + \mu \left(\frac{\sum_j x_j^2(t)}{N} - 1 \right) x_i(t) \right] dt + i \int \tilde{x}_i(t) [\dot{x}_i(t) - v_i(t)] dt \right\} \times \quad (\text{A8})$$

$$\times \exp \left\{ - \int \frac{1}{2} Q'[C_x(t, t')] \sum_j i \tilde{v}_j(t) i \tilde{v}_j(t') dt' dt - \int Q''[C_x(t, t')] R_{x|v}(t, t') \sum_j i \tilde{v}_j(t') x_j(t) dt' dt \right\}. \quad (\text{A9})$$

Finally we can take a Hubbard-Stratonovich transform on the first term of the second line and identify a stochastic process $\Xi(t)$ with zero mean at all times and covariance $\mathbb{E}[\Xi(t)\Xi(t')] = Q'[C_x(t, t')]$. The resulting generating functional now represent the dynamics in \mathbf{x} and \mathbf{v} where the cross-element interactions are replaced by the stochastic process. The resulting effective equations are

$$m\dot{\mathbf{v}}(t) = -\mathbf{v}(t) + \int_0^t dt'' R_{x|v}(t, t'') Q'[C_x(t, t'')] \mathbf{x}(t'') + \Xi(t) - \mu [C_x(t, t) - 1] \mathbf{x}(t), \quad (\text{A10})$$

$$\dot{\mathbf{x}}(t) = \mathbf{v}(t). \quad (\text{A11})$$

Finally we introduce the order parameters Eqs. (25-29) and compute their equation explicitly by substituting the equations of the effective dynamics. In order to do that, we use Girsanov theorem and evaluate the following expected values

$$\langle v(t)\Xi(t') \rangle = \int_0^{t'} dt'' R_v(t, t'') Q'[C_x(t, t'')], \quad (\text{A12})$$

$$\langle x(t)\Xi(t') \rangle = \int_0^{t'} dt'' R_{x|v}(t, t'') Q'[C_x(t, t'')]. \quad (\text{A13})$$

The dynamical equations are

$$\partial_t C_x(t, t') = C_{xv}(t', t); \quad (\text{A14})$$

$$m\partial_t C_v(t, t') = -C_v(t, t') + \int_0^t dt'' R_{x|v}(t, t'') Q''[C_x(t, t'')] C_{xv}(t'', t') + \int_0^{t'} Q'[C_x(t, t'')] R_v(t', t'') + \\ - \mu C_x(t, t') (C_x(t, t') - 1); \quad (\text{A15})$$

$$\partial_t C_{xv}(t, t') = C_v(t, t'); \quad (\text{A16})$$

$$m\partial_t C_{xv}(t, t') = -C_{xv}(t, t') + \int_0^{t'} dt'' R_{x|v}(t', t'') Q''[C_x(t', t'')] C_x(t, t'') + \int_0^t Q'[C_x(t', t'')] R_{x|v}(t, t'') + \\ - \mu C_{xv}(t, t') (C_x(t, t') - 1); \quad (\text{A17})$$

$$m\partial_t R_v(t, t') = \delta(t - t') - R_v(t, t') + \int_{t'}^t dt'' Q''[C(t, t'')] R_{x|v}(t, t'') R_{x|v}(t'', t') + -\mu R_{x|v}(t, t') (C_x(t, t') - 1); \quad (\text{A18})$$

$$\partial_t R_{x|v}(t, t') = R_v(t, t'). \quad (\text{A19})$$

and $\mu(t) = C_{xv}(t, t)$.

The initial conditions are :

$$C_x(t, t) = 1; \quad (\text{A20})$$

$$C_v(t = 0, t = 0) = 0; \quad (\text{A21})$$

$$C_{xv}(t = 0, t = 0) = 0; \quad (\text{A22})$$

$$R_v(t^+, t^+) = 1/m; \quad (\text{A23})$$

$$R_{x|v}(t, t) = 0. \quad (\text{A24})$$

Where Eq. (A20) comes from the spherical constraint; Eqs. (A21,A22) come from the initialization with no kinetic energy $\mathbf{v}(0) = \mathbf{0}$; Eqs. (A23) and (A24) come from Eqs. (A10) and (A11) (respectively) after deriving by $\Xi(t')$, integrating on t in $[t-h; t+h]$ (with $h \rightarrow 0$) and taking $t' \rightarrow t$. The equations shown in the main text are the discrete equivalent of the ones just obtained.

Appendix B: Spiked matrix-tensor model

In this section we discuss how the DMFT equations of the spiked matrix-tensor model differ from the mixed p -spin model. The main difference is that the hidden solution deforms locally the loss function

$$\begin{aligned} \mathcal{H} = & -\frac{1}{\Delta_p} \sqrt{\frac{(p-1)!}{N^{p-1}}} \sum_{i_1, \dots, i_p=1}^N T_{i_1, \dots, i_p} x_{i_1} \dots x_{i_p} - \frac{1}{\Delta_2} \frac{1}{\sqrt{N}} \sum_{i,j=1}^N Y_{ij} x_i x_j + \\ & - \frac{1}{p\Delta_p} \left(\frac{1}{N} \sum_j x_j x_j^* \right)^p - \frac{1}{2\Delta_2} \left(\frac{1}{N} \sum_j x_j x_j^* \right)^2 + \frac{\mu}{4N} \left(\sum_{i=1}^N x_i^2 - N \right)^2. \end{aligned} \quad (\text{B1})$$

As it clearly appears from the equation of the loss, the overlap of the hidden solution with the estimator plays an important role. This leads to two additional order parameters $m_x[t] = \frac{1}{N} \sum_j x_j[t] x_j^*$ and $m_y[t] = \frac{1}{N} \sum_j y_j[t] x_j^*$ (or $m_v(t) = \frac{1}{N} \sum_j v_j(t) x_j^*$ for massive gradient flow).

Since the stochastic part of the loss is unchanged, the steps shown in section IV of the main text and section A in the SI apply. They lead to modified dynamical equation where overlap with the hidden solution is present, for instance in Nesterov they are

$$\begin{aligned} x_0[t+1] = & y_0[t] + \alpha \Xi[t] - \alpha \mu (C_y[t, t] - 1) y_0[t] + \\ & + \alpha^2 \sum_{t''=0}^t R_y[t, t''] Q''(C_y[t, t'']) y_0[t''] + Q'(m_y[t]) \mathbf{x}^*, \end{aligned} \quad (\text{B2})$$

$$y_0[t+1] = x_0[t+1] + \frac{t}{t+3} (x_0[t+1] - x_0[t]). \quad (\text{B3})$$

Finally, substituting the effective dynamics into the definition of the order parameters we obtain:

• for Nesterov acceleration

$$\begin{aligned} C_x[t+1, t'] = & C_{xy}[t, t'] + \alpha^2 \sum_{t''=0}^{t'} R_x[t', t''] Q'(C_y[t, t'']) + \alpha^2 \sum_{t''=0}^t R_y[t, t''] Q''(C_y[t, t'']) C_{xy}[t', t''] + \\ & - \alpha \mu (C_y[t, t] - 1) C_y[t, t'] - Q'(m_y[t]) m_x[t'], \end{aligned} \quad (\text{B4})$$

$$\begin{aligned} C_{xy}[t+1, t'] = & C_y[t, t'] + \alpha^2 \sum_{t''=0}^{t'} R_y[t', t''] Q'(C_y[t, t'']) + \alpha^2 \sum_{t''=0}^t R_y[t, t''] Q''(C_y[t, t'']) C_y[t', t''] + \\ & - \alpha \mu (C_y[t, t] - 1) C_{xy}[t, t'] - Q'(m_y[t]) m_y[t'], \end{aligned} \quad (\text{B5})$$

$$C_{xy}[t', t+1] = C_x[t+1, t'] + \frac{t}{t+3} (C_x[t+1, t'] - C_x[t, t']), \quad (\text{B6})$$

$$C_y[t', t+1] = C_{xy}[t+1, t'] + \frac{t}{t+3} (C_{xy}[t+1, t'] - C_{xy}[t, t']), \quad (\text{B7})$$

$$R_x[t+1, t'] = R_y[t, t'] + \delta_{t, t'} + \alpha^2 \sum_{t''=t'}^t R_y[t, t''] R_y[t'', t'] Q''(C_y[t, t'']) - \alpha \mu (C_y[t, t] - 1) R_y[t, t'], \quad (\text{B8})$$

$$R_y[t', t+1] = R_x[t+1, t'] + \frac{t}{t+3} (R_x[t+1, t'] - R_x[t, t']), \quad (\text{B9})$$

$$m_x[t+1] = m_y[t] - \alpha \mu (C_y[t, t] - 1) m_y[t] + \alpha^2 \sum_{t''=0}^t R_y[t, t''] Q''(C_y[t, t'']) m_y[t''] + Q'(m_y[t]), \quad (\text{B10})$$

$$m_y[t+1] = m_x[t+1] + \frac{t}{t+3} (m_x[t+1] - m_x[t]), \quad (\text{B11})$$

with initial conditions $C_x[0,0] = 1$, $C_y[0,0] = 1$, $C_{xy}[0,0] = 1$, $R_x[t+1,t] = 1$, $R_y[t+1,t] = \frac{2t+3}{t+3}$, $m_x[0] = 0^+$, $m_y[0] = 0^+$;

• for massive gradient flow

$$\partial_t C_x(t, t') = C_{xv}(t', t), \quad (\text{B12})$$

$$\begin{aligned} m \partial_t C_v(t, t') = & -C_v(t, t') + \int_0^t dt'' R_{x|v}(t, t'') Q''[C_x(t, t'')] C_{xv}(t'', t') + \int_0^{t'} Q'[C_x(t, t'')] R_v(t', t'') + \\ & - \mu C_x(t, t') (C_x(t, t) - 1) + Q'[m_x(t')] m_x(t), \end{aligned} \quad (\text{B13})$$

$$\partial_t C_{xv}(t, t') = C_v(t, t'), \quad (\text{B14})$$

$$\begin{aligned} m \partial_t' C_{xv}(t, t') = & -C_{xv}(t, t') + \int_0^{t'} dt'' R_{x|v}(t', t'') Q''[C_x(t', t'')] C_x(t, t'') + \int_0^t Q'[C_x(t', t'')] R_{x|v}(t, t'') + \\ & - \mu C_{xv}(t, t') (C_x(t, t) - 1) + Q'[m_x(t')] m_v(t'), \end{aligned} \quad (\text{B15})$$

$$m \partial_t R_v(t, t') = \delta(t - t') - R_v(t, t') + \int_{t'}^t dt'' Q''[C(t, t'')] R_{x|v}(t, t'') R_{x|v}(t'', t') - \mu R_{x|v}(t, t') (C_x(t, t) - 1), \quad (\text{B16})$$

$$\partial_t R_{x|v}(t, t') = R_v(t, t'), \quad (\text{B17})$$

$$\partial_t m_x(t) = m_v(t), \quad (\text{B18})$$

$$m \partial_t m_v(t) = -m_v(t) + \int_0^t dt'' R_{x|v}(t, t'') Q''[C_x(t, t'')] m_x(t'') + Q'[m_x(t)] - \mu m_x(t) (C_x(t, t) - 1), \quad (\text{B19})$$

with initial conditions are : $C_x(0,0) = 1$; $C_v(0,0) = 0$; $C_{xv}(0,0) = 0$; $R_v(t^+, t) = 1/m$; $R_{x|v}(t, t) = 0$; $m_x(0) = 0^+$. $m_y(0) = 0^+$.

Finally the equation to compute the loss in time is

$$\mathcal{L}[t] = -\frac{\alpha}{\Delta_p} \sum_{t''=0}^t R_x[t, t'] C_x[t, t']^{p-1} / C_x[t, t]^{\frac{p}{2}} - \frac{\alpha}{\Delta_2} \sum_{t''=0}^t R_x[t, t'] C_x[t, t'] / C_x[t, t] - Q(m_x[t]). \quad (\text{B20})$$

Appendix C: Hard spherical constraint

It is also possible to consider a hard spherical constraint, which is the situation typically considered in the physics literature [11, 13]. A massive dynamics was already considered in [14] but their derivation was in the underdamped regime where the total energy is conserved. Using that approach the conservation of the energy was key. Unfortunately the energy is not conserved in general, and in particular in the case of optimization where we aim to go down in energy in order to find a minimum.

For reference sake we consider massive gradient flow, the same considerations apply straightforwardly to Nesterov acceleration. Let us write the dynamics in this case splitting the system in two ODEs

$$m \dot{\mathbf{v}}(t) = -\mathbf{v}(t) - \nabla \mathcal{L}[\mathbf{x}(t)], \quad (\text{C1})$$

$$\dot{\mathbf{x}}(t) = \mathbf{v}(t) - \mu(t) \mathbf{x}(t). \quad (\text{C2})$$

The last term in the second line constraints the dynamics to move in the sphere by removing the terms of the velocity that move orthogonally to the sphere. Therefore the term $\mu(t)$ is given by the projection of the velocity in the direction that is tangent to the sphere $\sum_j x_j(t) v_j(t) / N$.

We can then follow the usual techniques, e.g. section A, and obtain

$$\partial_t C_x(t, t') = -\mu(t) C_x(t, t') + C_{xv}(t', t), \quad (\text{C3})$$

$$m \partial_t C_v(t, t') = -C_v(t, t') + \int_0^t dt'' R_{x|v}(t, t'') Q''[C_x(t, t'')] C_{xv}(t'', t') + \int_0^{t'} Q'[C_x(t, t'')] R_v(t', t''), \quad (\text{C4})$$

$$\partial_t C_{xv}(t, t') = -\mu(t) C_{xv}(t, t') + C_v(t, t') , \quad (\text{C5})$$

$$m \partial_{t'} C_{xv}(t, t') = -C_{xv}(t, t') + \int_0^{t'} dt'' R_{x|v}(t', t'') Q'' [C_x(t', t'')] C_x(t, t'') + \int_0^t Q' [C_x(t', t'')] R_{x|v}(t, t'') , \quad (\text{C6})$$

$$m \partial_t R_v(t, t') = \delta(t - t') - R_v(t, t') + \int_{t'}^t dt'' Q'' [C(t, t'')] R_{x|v}(t, t'') R_{x|v}(t'', t') , \quad (\text{C7})$$

$$\partial_t R_{x|v}(t, t') = -\mu(t) R_{x|v}(t, t') + R_v(t, t'); \quad (\text{C8})$$

with $\mu(t) = C_{xv}(t, t)$ and initial conditions $C_x(t, t) = 1$, $C_v(0, 0) = 0$, $C_{xv}(0, 0) = 0$, $R_v(t^+, t) = \frac{1}{m}$, $R_{x|v}(t, t) = 0$.